Jung et al. Nanoscale Research Letters (2019) 14:278
https://doi.org/10.1186/s11671-019-3119-3

Nanoscale Research Letters

NANO EXPRESS Open Access

Effect of Ultraviolet-Ozone Treatment on MoS_2 Monolayers: Comparison of Chemical-Vapor-Deposited Polycrystalline Thin Films and Mechanically Exfoliated Single Crystal Flakes

Changki Jung, Hae In Yang and Woong Choi*

Abstract

We report the different oxidation behavior between polycrystalline chemical-vapor-deposited and mechanically exfoliated single crystal MoS_2 monolayers by ultraviolet-ozone treatment. As ultraviolet-ozone treatment time increased from 0 to 5 min, photoluminescence emission and Raman modes of both MoS_2 disappeared, suggesting structural degradation by oxidation. Analysis with optical absorbance and X-ray photoelectron spectroscopy suggested the formation of MoO_3 in both MoS_2 after ultraviolet-ozone treatment. In addition, ultraviolet-ozone treatment possibly led to the formation of oxygen vacancies, molybdenum oxysulfide, or molybdenum sulfates in chemical-vapor-deposited MoS_2. The measurement of electrical resistance after ultraviolet-ozone treatment suggested the transformation of chemical-vapor-deposited MoS_2 into doped MoO_3 and of mechanically exfoliated MoS_2 into negligibly doped MoO_3. These results demonstrate that the crystallinity of monolayer MoS_2 can strongly influence the effect of ultraviolet-ozone treatment, providing important implications on the device integration of MoS_2 and other two-dimensional semiconductors.

Keywords: MoS_2, Monolayer, Single crystal, Polycrystalline, UV-O_3 treatment

Introduction

There is a great interest in transition metal dichalcogenides (TMDs), such as MoS_2, since they offer an attractive possibility for various device applications including transistors, optoelectronic devices, heterojunction structures, sensors, and electrocatalysis [1, 2]. The existence of direct bandgaps in monolayer TMDs makes these two-dimensional semiconductors especially promising for optoelectronic devices [3, 4]. However, critical challenges to fabricate TMD-based optoelectronic devices such as phototransistors include the deposition of high-*k* dielectrics on TMDs and the doping of TMDs. Because of the absence of dangling bonds on the surface of TMDs, it is challenging to deposit high-*k* dielectrics on TMDs [5]. Moreover, the doping of TMDs is also challenging as the substitutional doping used for bulk semiconductors such as silicon modifies the two-dimensional structure and properties of monolayer TMDs [6].

To overcome these difficulties, surface functionalization of TMDs by O_2 plasma [7, 8] or ultraviolet-ozone (UV-O_3) [9–11] has been suggested. While these methods can functionalize the surface of MoS_2 by surface oxidation, they can simultaneously influence the structure and properties of monolayer MoS_2 [12–16]. For example, oxidation by O_2 plasma or UV-O_3 treatment altered the Raman vibration modes and photoluminescence (PL) emission of monolayer MoS_2 [12, 16]. However, as most studies were based on micrometer-scale monolayer MoS_2 flakes obtained by mechanical exfoliation from bulk single crystals, little has been known on their interaction with large-area monolayer MoS_2 thin films, which are typically polycrystalline. Grain boundaries in polycrystalline monolayer

* Correspondence: woongchoi@kookmin.ac.kr
School of Materials Science & Engineering, Kookmin University, Seoul 02707, South Korea

MoS_2 may allow higher reactivity with UV-O_3 than that of single crystal, resulting in different oxidation behavior. Therefore, in this study, we explore the effect of UV-O_3 treatment on MoS_2 monolayers by directly comparing the oxidation behavior of polycrystalline chemical vapor deposition (CVD) thin films and mechanically exfoliated single crystal flakes. We systematically investigate the PL and Raman spectra of both MoS_2 monolayers for different duration of UV-O_3 exposure. We also investigate the oxidation behavior of both MoS_2 monolayers during UV-O_3 treatment with X-ray photoelectron spectroscopy (XPS). We further measure electrical resistance of pristine and UV-O_3-treated MoS_2 monolayers to understand the effect of UV-O_3 treatment on MoS_2 monolayers.

Methods

Monolayer MoS_2 thin films were deposited on (0001)-oriented sapphire substrates (~ 1.5 × 1 cm^2) by CVD in a two-zone tube furnace. MoO_3 (99.98%, Sigma-Aldrich) and S (99.98%, Sigma-Aldrich) powders in two separate Al_2O_3 boats were used as precursors. MoO_3 powder (14 mg) was placed upstream at zone 1 (750 °C) and S powder (1.4 g) was placed at the upstream entry of the furnace. Substrates were placed downstream at zone 2 (700 °C). MoO_3 powder was heated at a rate of 15 °C min^{-1} and substrates were heated at 38 °C min^{-1}. After 30-min deposition, the furnace was slowly cooled down to room temperature. Ar flow of 100 sccm and a pressure of ~ 0.5 Torr were maintained during deposition. Monolayer MoS_2 flakes were obtained by the gold-mediated exfoliation method [17] from bulk MoS_2 crystals (2D Semiconductors) and transferred on highly-doped Si substrates with thermally grown SiO_2 (300 nm). Figure 1 shows schematic structures of both MoS_2 monolayers on substrates. The thickness of monolayer MoS_2 was measured using atomic force microscopy (AFM, Park Systems XE-100). The crystallinity of bulk MoS_2 crystals and CVD MoS_2 thin films was investigated by X-ray diffraction (XRD, Bruker D8 Discover with Cu-Kα radiation) and transmission electron microscopy (TEM, FEI Titan 80–300 at 300 kV), respectively.

MoS_2 monolayers were exposed to UV-O_3 (SEN LIGHTS PL16–110, 185 nm and 254 nm) for 0–5 min at the irradiance of 58 mW cm^{-2}. Optical absorbance was measured by UV-visible spectroscopy (PerkinElmer Lambda 35). Raman/PL spectroscopy (Horiba Jobin-Yvon LabRam Aramis) were measured on pristine and UV-O_3-treated MoS_2 monolayers with a 532-nm laser and a beam power of 0.5 mW. XPS (Thermo Scientific K-Alpha) was carried out using a monochromatic Al K_α x-ray source ($h\nu$ = 1486.7 eV) with a take-off angle of 45°, a pass energy of 40 eV, and a spot size of 400 μm in diameter. For all samples, C 1s and O 1s were observed presumably because they are exposed to atmosphere before loaded to ultrahigh vacuum chamber for XPS analysis. Adventitious carbon (C 1s at 284.8 eV) was used as a charge correction reference for XPS spectra. The energy resolution is 0.7 eV measured using the full width at half-maximum intensity of the Ag $3d_{5/2}$ peak. MoS_2 samples were exposed to atmosphere while they were brought to XPS equipment. Although in situ XPS analysis could provide more accurate information, it was unavailable in this work. For peak deconvolution and background subtraction, Thermo Scientific Avantage Data System software was used. Gaussian functions were used to fit XPS spectra.

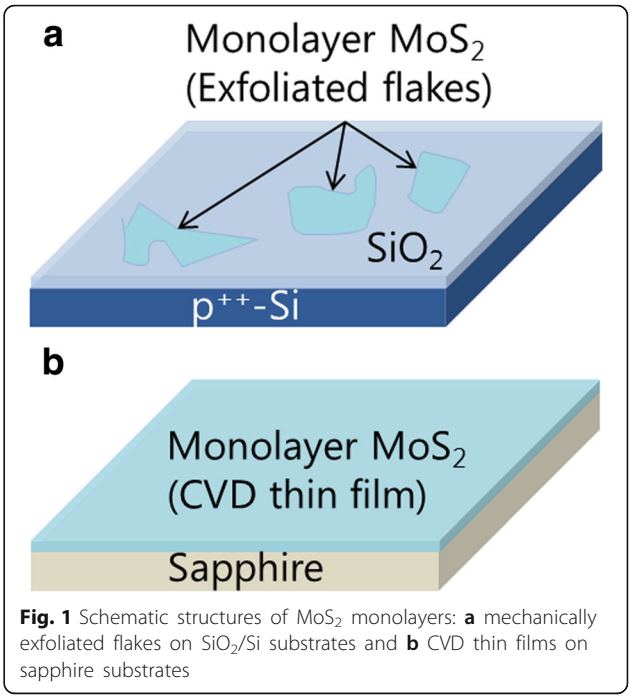

Fig. 1 Schematic structures of MoS_2 monolayers: **a** mechanically exfoliated flakes on SiO_2/Si substrates and **b** CVD thin films on sapphire substrates

To measure the electrical resistance of MoS_2 monolayers, Au contacts (100 × 100 μm^2, 70 nm thick) were deposited on top of MoS_2 by electron-beam evaporation. Spin-coated photoresist on top of Au layer was then patterned by conventional photolithography to form opening areas for subsequent etching. After Au in opening areas was removed by wet etching in aqua regia, remaining photoresist was removed in acetone. Then, the devices were annealed at 200 °C for 2 h in a tube furnace (100 sccm Ar and 10 sccm H_2) to remove photoresist residue and to decrease contact resistance. Electrical resistance was calculated with current-voltage (I–V) measurement (Keithley 4200-SCS) in atmospheric environments.

Results and Discussion

Beside AFM measurement, PL and Raman spectra are measured to confirm the formation of MoS_2 monolayers. Because of its direct bandgap, MoS_2 monolayers allow PL emission at ~ 1.88 eV [3, 4]. In addition, the frequency difference between the two characteristic Raman A_{1g} and E^1_{2g} modes of MoS_2 monolayers is less than 20 cm^{-1} [18]. In Fig. 3, the PL emission of pristine MoS_2 at ~ 1.88 eV indicates that both MoS_2 are monolayers. In Fig. 4, pristine MoS_2 exhibits the frequency difference between 19.6 and 19.9 cm^{-1} implying monolayer MoS_2. XRD and TEM analysis indicated the single crystal nature of bulk MoS_2 crystals and polycrystalline nature of our monolayer MoS_2 thin films (Additional file 1: Figure S1). The grain size of monolayer MoS_2 thin films is ~ 10 nm [19].

After UV-O_3 treatment, MoS_2 monolayers change their color and become transparent. In Fig. 2a, b, both exfoliated flakes and CVD thin films become transparent after 5-min UV-O_3 treatment. The absorbance spectrum of MoS_2 thin films in Fig. 2c clearly shows the difference after UV-O_3 treatment. (The absorbance of exfoliated MoS_2 flakes could not be measured with UV-visible spectroscopy as the size of flakes was too small.) While pristine MoS_2 thin films show absorbance peaks due to excitonic transitions (A and B) [3, 4], 5-min UV-O_3-treated MoS_2 thin films do not exhibit any absorbance peaks at all for the same range of wavelength. Because lightly yellow-green MoS_2 thin films become transparent to visible light after 5-min UV-O_3 treatment, we expect the energy bandgap of pristine monolayer MoS_2 (~ 1.88 eV) to become wider after UV-O_3 treatment (> ~ 3 eV). As this is in good agreement with the wide bandgap of MoO_3 (> 2.7 eV) [20], the transparent UV-O_3-treated MoS_2 suggests the formation of MoO_3 after 5-min UV-O_3 treatment.

We then investigate the effect of UV-O_3 treatment on the PL emission of MoS_2 monolayers. Figure 3 shows the PL spectra of CVD MoS_2 thin films and exfoliated MoS_2 single crystal flakes after UV-O_3 exposure for 0, 1,

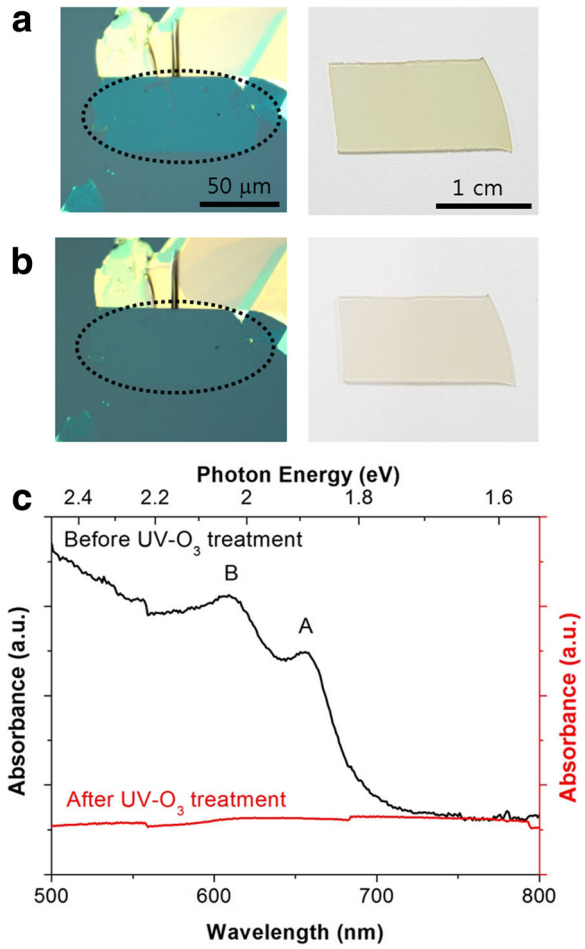

Fig. 2 Mechanically exfoliated flakes and CVD thin films of MoS_2 monolayers **a** before and **b** after 5-min UV-O_3 treatment (dotted region indicates monolayer), **c** optical absorbance of CVD thin films before and after 5-min UV-O_3 treatment

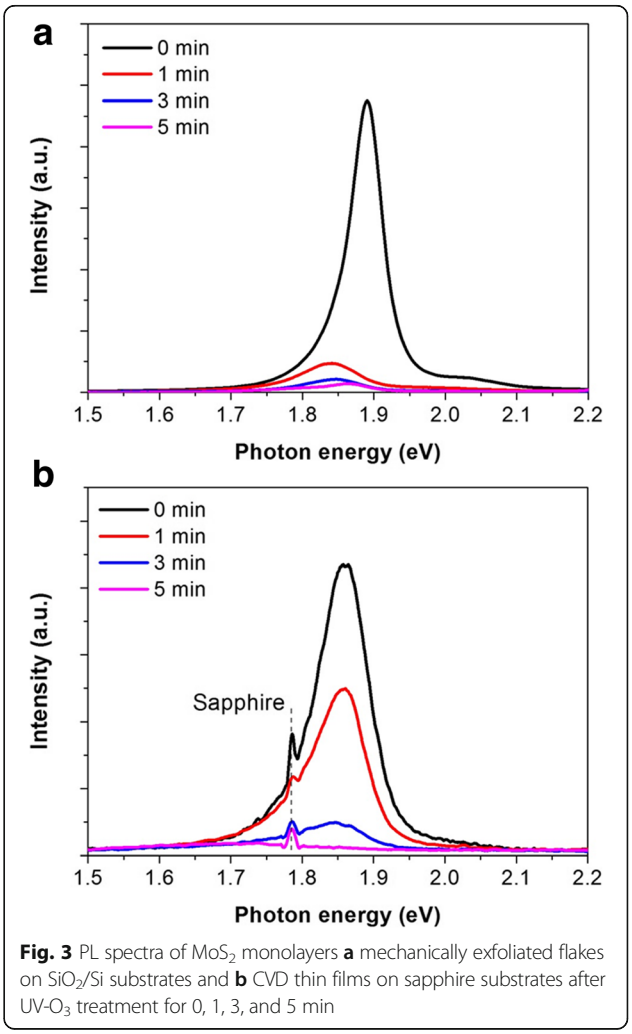

Fig. 3 PL spectra of MoS_2 monolayers **a** mechanically exfoliated flakes on SiO_2/Si substrates and **b** CVD thin films on sapphire substrates after UV-O_3 treatment for 0, 1, 3, and 5 min

3, and 5 min, respectively. The intensity of PL emission decreases significantly with UV-O_3 treatment time and eventually PL is fully quenched for the 5-min-treated MoS_2 monolayers. These results suggest the formation of oxides or defects allowing non-radiative recombination after UV-O_3 treatment. As MoS_2 monolayers become transparent after UV-O_3 treatment, the formation of wide bandgap semiconductor MoO_3 is reasonably expected. The energy of PL emission of pristine MoS_2 is 1.88 eV for exfoliated flakes and 1.86 eV for CVD films. This slight difference is probably due to the effect of underlying substrates as substrates can strongly influence the Raman and PL emission [21]. The wider width of PL emission peak in CVD monolayers suggests higher defect density. Interestingly, further negative shift of PL emission peak is observed in single crystal MoS_2 flakes (~ 50 meV) than in CVD thin films (by ~ 10 meV) after UV-O_3 treatment. As the negative shift of PL emission is comparable with trion binding energy (10–40 meV) of MoS_2 [22], this may be due to different concentrations of trion (neutral excitons accepting an electron or a hole) formed by oxidation-induced doping [23, 24]. (In this work, single crystal MoS_2 flake is more conductive than CVD MoS_2, suggesting higher doping levels in single crystal MoS_2.) The higher doping level in single crystal MoS_2 flakes will allow high concentration of trions, of which recombination will dominate their PL emission. In contrast, the lower doping level in CVD MoS_2 thin films will allow low concentration of trions. Hence, their PL emission will be dominated by the recombination of neutral excitons. However, as the negative shift of PL emission may also be related to the effect of underlying substrates or strains, more systematic investigation is needed in the future.

Next, to investigate the structural degradation by UV-O_3 treatment, we measure the Raman spectra of MoS_2 monolayers after UV-O_3 treatment for 0, 1, 3, and 5 min, respectively (Fig. 4). The intensity of both E^1_{2g} and A_{1g} modes decreases as the treatment time increases. While the frequency difference between E^1_{2g} and A_{1g} modes remains unchanged for 0–5 min of UV-O_3 treatment time, the two Raman modes almost completely disappear after 5-min treatment, suggesting severe structural distortion and degradation. AFM analysis indicates an increase of surface roughness after UV-O_3 treatment (Additional file 1: Figure S2), which is consistent with the oxidation of MoS_2 [23].

To further investigate the structural degradation of MoS_2 monolayers by UV-O_3 treatment, we measure XPS spectra of MoS_2. Because the beam size of XPS is much larger than the size of single-layer MoS_2 flakes, XPS spectra for single crystal MoS_2 flakes are obtained from large-area MoS_2 single crystals (~ 1 cm in size and ~ 100 μm in thickness). Figure 5 shows the XPS spectra in

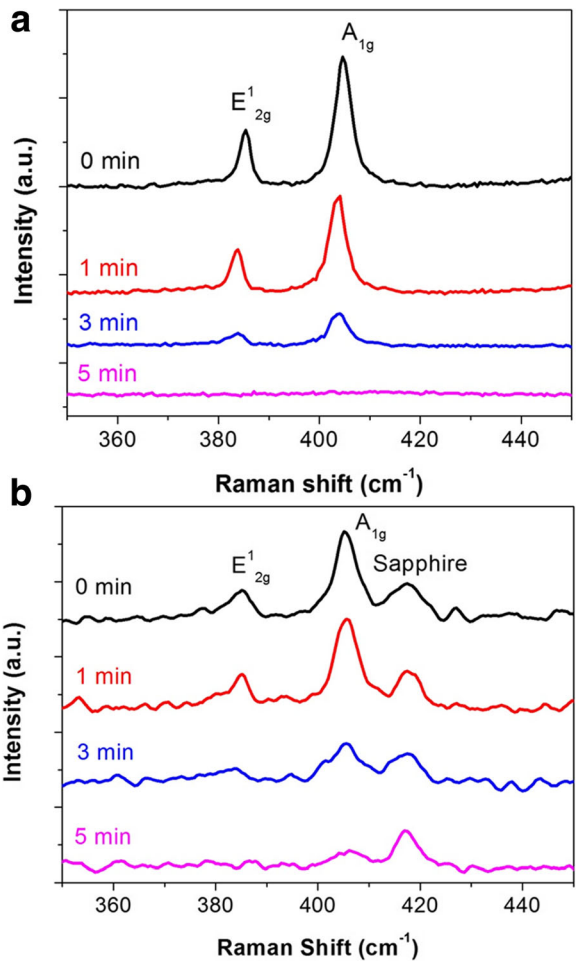

Fig. 4 Raman spectra of MoS_2 monolayers **a** mechanically exfoliated flakes on SiO_2/Si substrates and **b** CVD thin films on sapphire substrates after UV-O_3 treatment for 0, 1, 3, and 5 min

Mo 3d and S 2p regions for bulk single crystal and CVD MoS_2 thin films, respectively. The existence of Mo^{4+}-state of pristine MoS_2 can be observed from the binding energy of Mo $3d_{3/2}$ and Mo $3d_{5/2}$ orbitals. After UV-O_3 exposure, the intensity of Mo^{6+}-state at 235.9 eV further increases with UV-O_3 treatment time indicating the expanded formation of Mo-O bonding and MoO_3. There are four distinct differences between Fig. 5a and b in Mo 3d region. (1) In Fig. 5b, Mo^{6+}-state at 235.9 eV in pristine MoS_2 thin films is probably due to residual oxide formed during or after CVD process. (2) The intensity of Mo^{4+} and S 2 s peaks decrease in CVD MoS_2 thin films with longer UV-O_3 exposure. However, the intensity of Mo^{4+} and S 2 s peaks does not change with UV-O_3 treatment time in large MoS_2 single crystals as XPS can still detect Mo^{4+} and S 2 s peaks from MoS_2 underneath the oxidized top surface. (3) In single crystal MoS_2, the binding energy of Mo^{4+}-state shows further positive shift than that in CVD MoS_2 thin films

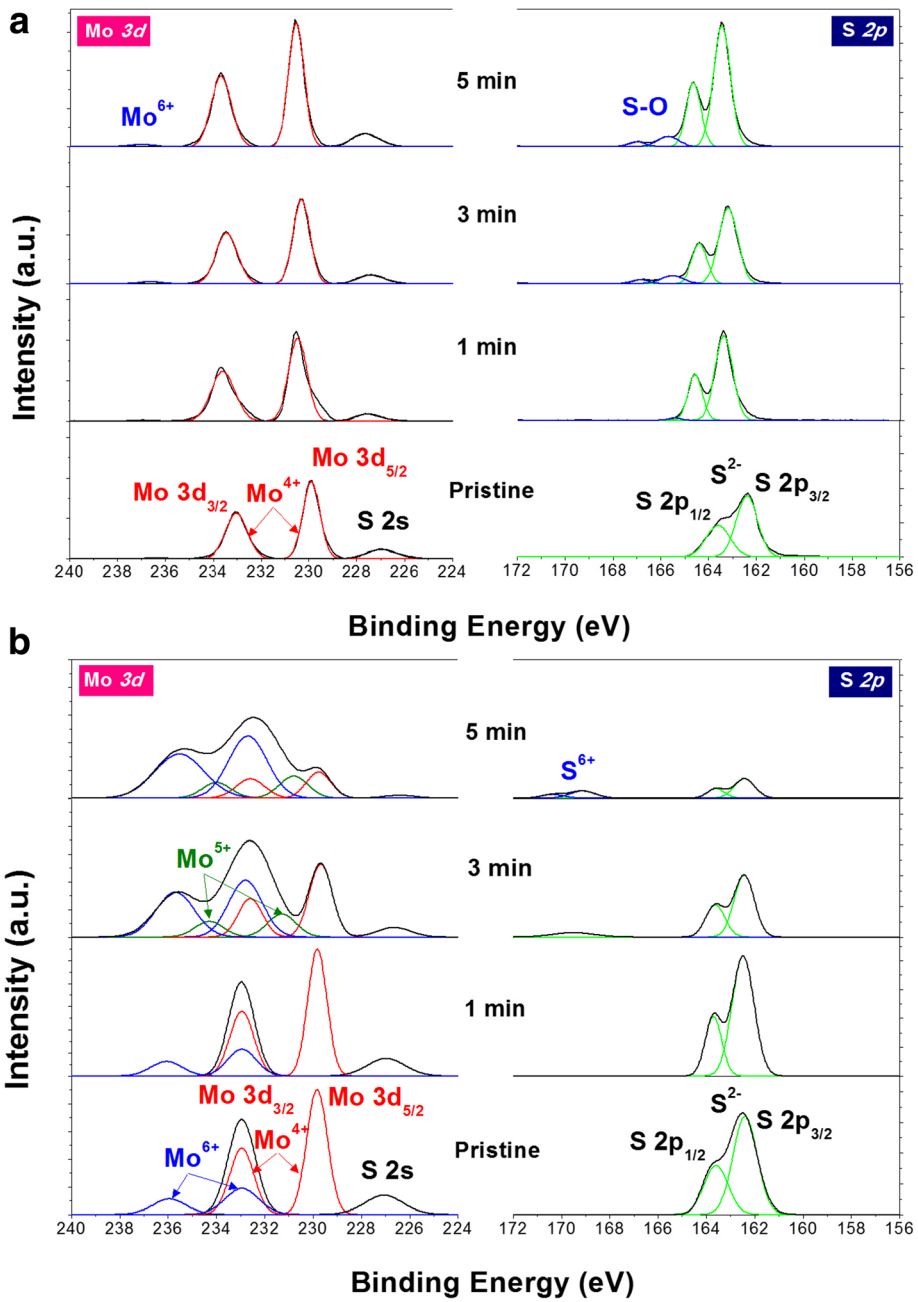

Fig. 5 XPS spectra of MoS_2 **a** bulk single crystal and **b** CVD thin films on sapphire substrates after UV-O_3 treatment for 0, 1, 3, and 5 min

suggesting higher n-type doping [25]. The peak shift after the oxidation of MoS_2 in this work (0.41–1.09 eV) is comparable to that in literature (0.6–1.1 eV) [23, 24]. (To prevent charging effect, which may induce similar positive shift, we used a flood gun during XPS measurement.) (4) In CVD MoS_2 thin films, the peaks of Mo^{5+}-state also appear with UV-O_3 treatment suggesting possibly the formation of oxygen vacancies [26] or molybdenum oxysulfide MoO_xS_y [27]. These results can be understood by the oxidation of Mo^{4+}-state in MoS_2 into higher oxidation states (Mo^{5+} and Mo^{6+}) with UV-O_3 exposure. This is also consistent with the XPS results on polycrystalline multilayer MoS_2 thin films after O_2 plasma or UV-O_3 treatment [26, 28, 29].

In S 2p region, the existence of S^{2-}-state can be observed from the binding energy of S $2p_{1/2}$ and S $2p_{3/2}$ orbitals in pristine MoS_2. The binding energy of S^{2-}-state in single crystal MoS_2 shows further positive shift than that in CVD MoS_2 thin films suggesting higher n-type doping [25]. Although S-O bond is observed at ~

165 eV in UV-O_3-treated single crystal MoS_2, it is below the detection limit in CVD thin films. Instead, a new doublet peak of sulfur oxidation state appears at higher binding energy (~ 169 eV) in CVD thin films after UV-O_3 treatment for 3 min. This new doublet corresponds to the S 2p peaks of oxidized sulfur S^{6+}, suggesting possibly the formation of various molybdenum sulfates Mo $(SO_4)_x$ [28]. While the intensity of S^{2-} doublet keeps decreasing with longer UV-O_3 exposure, the intensity of S^{6+} doublet further increases after 5-min UV-O_3 treatment, suggesting further conversion of S^{2-} into higher oxidation state (S^{6+}) by oxidation. Similarly with Mo^{4+} peaks, the intensity of S^{2-} peaks does not change with UV-O_3 treatment time in large MoS_2 single crystals. The existence of S^{6+}-state after O_2 plasma or UV-O_3 treatment is inconsistent in literature. Its existence was reported in polycrystalline multilayer MoS_2 thin films after O_2 plasma treatment [28]. However, it was not observed in other polycrystalline multilayer MoS_2 thin films [26, 29] or single crystals [9, 16, 30] after O_2 plasma or UV-O_3 treatment. While this inconsistency may be related to dose- and time-dependence of MoS_2 oxidation [30], more systematic investigation is needed to clarify this in the future.

The different XPS behavior may be related to the difference of composition and crystallinity between single crystals and CVD thin films. The composition of Mo:S is 1:1.97 in bulk single crystals and 1:1.5 in CVD thin films, suggesting higher concentration of S vacancies in CVD thin films. The higher concentration of S vacancies, combined with the existence of grain boundaries in CVD thin films, may allow higher reactivity to oxygen than that in single crystals.

To further understand the oxidation of MoS_2 monolayers by UV-O_3 treatment, we measure the electrical resistance of pristine and UV-O_3-treated MoS_2 monolayers. Because there is sample-to-sample variation of electrical resistance, we use relative ratio of electrical resistance (R_{After}/R_{Before}), where R_{After} and R_{Before} are electrical resistance after and before UV-O_3 treatment, respectively. Figure 6 shows R_{After}/R_{Before} as a function of UV-O_3 treatment time. While R_{After}/R_{Before} of exfoliated MoS_2 single crystal flakes significantly increases with longer treatment time, R_{After}/R_{Before} of CVD MoS_2 thin films decreases with longer treatment time. These results suggest that MoO_3 formed by the UV-O_3 treatment of CVD MoS_2 thin films possesses higher doping level than that of MoS_2 single crystal flakes. This is supported by XPS analysis suggesting the possible existence of oxygen vacancies, MoO_xS_y, or Mo $(SO_4)_x$ in CVD MoS_2 monolayers. This is seemingly contradicting with the higher doping in single crystal MoS_2 suggested in Fig. 5a. However, as Fig. 5a is based on bulk single crystals, we cannot exclude the possibility that it does not provide accurate information of the top monolayer. Hence, surface oxidation of bulk MoS_2 single crystal may possibly provide doping only to MoS_2 single crystal underneath, transforming top surface region into negligibly doped MoO_3. Consistent with these results, electrical resistance also increased when monolayer

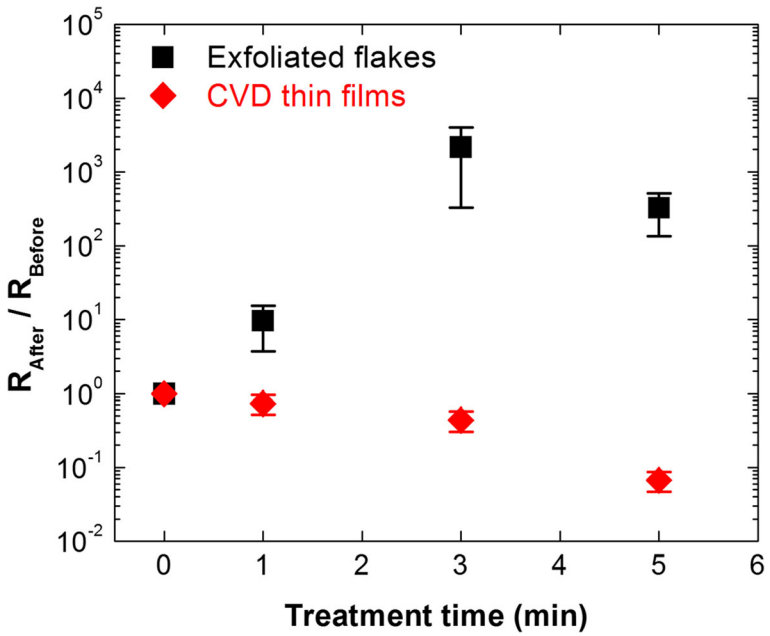

Fig. 6 Ratio of electrical resistance of MoS_2 monolayers as a function of UV-O_3 treatment time (R_{After}: electrical resistance after UV-O_3 treatment, R_{Before}: electrical resistance before UV-O_3 treatment)

MoS_2 single crystal flakes were oxidized by O_2 plasma [12]. As single crystal MoS_2 without grain boundaries could be more tolerant to oxidation than polycrystalline MoS_2, the effect of oxidation-induced doping may be stronger in polycrystalline MoS_2 than in single crystal MoS_2. However, further investigation is needed to understand this difference in the future.

Conclusions

In summary, we investigated the effect of UV-O_3 treatment on polycrystalline CVD thin films and single crystal flakes of monolayer MoS_2. Monolayer MoS_2 becomes transparent after UV-O_3 treatment suggesting the formation of wide bandgap semiconductor MoO_3. As UV-O_3 treatment time increases, the intensity of PL and Raman spectra significantly decreased, suggesting the formation of oxides or defects. In both MoS_2, XPS analysis indicated the formation of Mo-O bonds and MoO_3. However, in CVD MoS_2 thin films, the conversion of Mo^{4+}-and S^{2-}-states into Mo^{5+}- and S^{6+}-states was also observed after UV-O_3 treatment, suggesting the possible existence of oxygen vacancies, MoO_xS_y, or Mo $(SO_4)_x$. As the electrical resistance of single crystal MoS_2 monolayers significantly increased with longer UV-O_3 treatment time, the oxidation of single crystal MoS_2 into MoO_3 seems to provide negligible doping. In contrast, the electrical resistance of CVD MoS_2 monolayers decreased with longer UV-O_3 treatment time, suggesting that the oxidation of CVD MoS_2 into MoO_3 provides doping. These results demonstrate the significant impact of crystallinity on the effect of UV-O_3 treatment on MoS_2 monolayers, providing possibly interesting implications on fabricating heterojunction structures based on two-dimensional nanomaterials.

Additional File

Additional file 1: Crystallinity and AFM analysis. (DOCX 13198 kb)

Abbreviations

CVD: Chemical vapor deposition; I-V: Current-voltage; R_{After}: Resistance measured after ultraviolet-ozone treatment; R_{Before}: Resistance measured before ultraviolet-ozone treatment; TMDs: Transition metal dichalcogenides; UV-O_3: Ultraviolet-ozone; XPS: X-ray photoelectron spectroscopy

Acknowledgements

Not applicable

Authors' Contributions

CJ and HIY contributed equally to this work. WC initiated the research. CJ worked on the growth and characterization of CVD thin films. HIY worked on the fabrication and characterization of mechanically-exfoliated single-layer flakes. WC wrote the manuscript. All authors read and approved the manuscript.

Funding

This work was supported by the National Research Foundation of Korea (Grant NRF-2013K1A4A3055679, NRF-2016R1A2B4014369, and NRF-2019R1F1A1057293).

Availability of Data and Materials

All data and materials may be provided on a reasonable request.

Competing Interests

The authors declare that they have no competing interests.

Received: 11 April 2019 Accepted: 8 August 2019
Published online: 15 August 2019

References

1. Radisavljevic B, Radenovic A, Brivio J, Giacometti V, Kis A (2011) Single-layer MoS_2 transistors. Nat Nanotechnol 6:147–150
2. Kim S, Konar A, Hwang W-S, Lee JH, Lee J, Yang J, Jung C, Kim H, Yoo J-B, Choi J-Y, Jin YW, Lee SY, Jena D, Choi W, Kim K (2012) High-mobility and low-power thin-film transistors based on multilayer MoS_2 crystals. Nat Commun 3:1011
3. Splendiani A, Sun L, Zhang Y, Li T, Kim J, Chim C, Galli G, Wang F (2010) Emerging photoluminescence in monolayer MoS_2. Nano Lett 10:1271–1275
4. Mak KF, Lee C, Hone J, Shan J, Heinz TF (2010) Atomically thin MoS_2: a new direct-gap semiconductor. Phys Rev Lett 105:136805
5. Liu H, Xu K, Zhang X, Ye PD (2012) The integration of high-k dielectric on two-dimensional crystals by atomic layer deposition. Appl Phys Lett 100:152115
6. Allain A, Kang J, Banerjee K, Kis A (2015) Electrical contacts to two-dimensional semiconductors. Nat Mater 14:1195–1205
7. Yang J, Kim SK, Choi W, Park SH, Jung YK, Cho MH, Kim HS (2013) Improved growth behavior of atomic-layer-deposited high-k dielectrics on multilayer MoS_2 by oxygen plasma pretreatment. ACS Appl Mater Interfaces 5:4739–4744
8. Yang W, Sun Q-Q, Geng Y, Chen L, Zhou P, Ding S-J, Zhang DW (2015) The integration of Sub-10 nm gate oxide on MoS_2 with ultra low leakage and enhanced mobility. Sci Rep 5:11921
9. Azcatl A, McDonnell S, KC S, Peng X, Dong H, Qin X, Addou R, Mordi GI, Lu N, Kim J, Kim MJ, Cho K, Wallace RM (2014) MoS_2 functionalization for ultra-thin atomic layer deposited dielectrics. Appl Phys Lett 104:111601
10. Su W, Kumar N, Spencer SJ, Dai N, Roy D (2015) Transforming bilayer MoS_2 into single-layer with strong photoluminescence using UV-ozone oxidation. Nano Res 8:3878–3886
11. Wang J, Li S, Zou X, Ho J, Liao L, Xiao X, Jiang C, Hu W, Wang J, Li J (2015) Integration of high-k oxide on MoS_2 by using ozone pretreatment for high-performance MoS_2 top-gated transistor with thickness-dependent carrier scattering investigation. Small 11:5932–5938
12. Kang N, Paudel HP, Leuenberger MN, Tetard L, Khondaker SI (2014) Photoluminescence quenching in single-layer MoS_2 via oxygen plasma treatment. J Phys Chem C 118:21258–21263
13. Nan H, Wang Z, Wang W, Liang Z, Lu Y, Chen Q, He D, Tan P, Miao F, Wang X, Wang J, Ni Z (2014) Strong photoluminescence enhancement of MoS_2 through defect engineering and oxygen bonding. ACS Nano 8(6):5738–5745
14. Kim MS, Nam G, Park S, Kim H, Han GH, Lee J, Dhakal KP, Leem J-Y, Lee YH, Kim J (2015) Photoluminescence wavelength variation of monolayer MoS_2 by oxygen plasma treatment. Thin Solid Films 590:318–323
15. Park S, Kim SY, Choi Y, Kim M, Shin H, Kim J, Choi W (2016) Interface properties of atomic-layer-deposited Al_2O_3 thin films on ultraviolet/ozone-treated multilayer MoS_2 crystals. ACS Appl Mater Interfaces 8:11189–11193
16. Yang HI, Park S, Choi W (2018) Modification of the optoelectronic properties of two-dimensional MoS_2 crystals by ultraviolet-ozone treatment. Appl Surf Sci 443:91–96
17. Desai SB, Madhvapathy SR, Amani M, Kiriya D, Hettick M, Tosun M, Zhou Y, Dubey M, Ager JW III, Chrzan D, Javey A (2016) Gold-mediated exfoliation of ultralarge optoelectronically-perfect monolayers. Adv Mater 28:4053–4058
18. Lee C, Yan H, Brus LE, Heinz TF, Hone J, Ryu S (2010) Anomalous lattice vibrations of single- and few-layer MoS_2. ACS Nano 4:2695–2700
19. Baek SH, Choi Y, Choi W (2015) Large-area growth of uniform single-layer MoS_2 thin films by chemical vapor deposition. Nanoscale Res Lett 10:388
20. Balendhran S, Deng J, Ou JZ, Walia S, Scott J, Tang J, Wang KL, Field MR, Russo S, Zhuiykov S, Strano MS, Medhekar N, Sriram S, Bhaskaran M,

Kalantar-zadeh K (2013) Enhanced charge carrier mobility in two-dimensional high dielectric molybdenum oxide. Adv Mater 25:109–114
21. Buscema M, Steele GA, van der Zant HSJ, Castellanos-Gomez A (2014) The effect of the substrate on the Raman and photoluminescence emission of single-layer MoS_2. Nano Res 7:561–571
22. Mak KF, He K, Lee C, Lee GH, Hone J, Heinz TF, Shan J (2013) Tightly bound trions in monolayer MoS_2. Nat Mater 12:207–211
23. Chen M, Nam H, Wi S, Ji L, Ren X, Bian L, Lu S, Liang X (2013) Stable few-layer MoS_2 rectifying diodes formed by plasma-assisted doping. Appl Phys Lett 103:142110
24. Zhu H, Qin X, Cheng L, Azcatl A, Kim J, Wallace RM (2016) Remote plasma oxidation and atomic layer etching of MoS_2. ACS Appl Mater Interfaces 8: 19119–19126
25. Fang H, Tosun M, Seol G, Chang TC, Takei K, Guo J, Javey A (2013) Degenerate n-doping of few-layer transition metal dichalcogenides by potassium. Nano Lett 13:1991–1995
26. Ko TY, Jeong A, Kim W, Lee J, Kim Y, Lee JE, Ryu GH, Park K, Kim D, Lee Z, Lee MH, Lee C, Ryu S (2017) On-stack two-dimensional conversion of MoS_2 into MoO_3. 2D Mater 4:014003
27. Bessonov AA, Kirikova MN, Petukhov DI, Allen M, Ryhänen T, Bailey MJA (2015) Layered memristive and memcapacitive switches for printable electronics. Nat Mater 14:199–204
28. Brown NMD, Cui N, McKinley A (1998) An XPS study of the surface modification of natural MoS_2 following treatment in an RF-oxygen plasma. Appl Surf Sci 134:11–21
29. Kwon KC, Kim C, Le QV, Gim S, Jeon J-M, Ham JY, Lee J-L, Jang HW, Kim SY (2015) Synthesis of atomically thin transition metal disulfides for charge transport layers in optoelectronic devices. ACS Nano 9:4146–4155
30. Azcatl A, KC S, Peng X, Lu N, McDonnell S, Qin X, de Dios F, Addou R, Kim J, Kim MJ, Cho K, Wallace RM (2015) HfO_2 on UV–O_3 exposed transition metal dichalcogenides: interfacial reactions study. 2D Mater 2:014004

Publisher's Note